Frankfurt preprint UFTP–406
Columbia preprint CU–TP–733

Relativistic Hydrodynamics for Heavy–Ion Collisions: Freeze–Out and Particle Spectra[†]

Stefan Bernard, Joachim A. Maruhn, Walter Greiner

Institut für Theoretische Physik der J.W. Goethe–Universität
Robert–Mayer–Str. 10, D–60054 Frankfurt/M., Germany

Dirk H. Rischke[‡]

Physics Department, Pupin Physics Laboratories, Columbia University
538 W 120th Street, New York, NY 10027, U.S.A.

January 1996

Abstract

We investigate freeze–out in hydrodynamic models for relativistic heavy–ion collisions. In particular, instantaneous freeze–out across a hypersurface of constant temperature ("isothermal" freeze–out) is compared with that across a hypersurface at constant time in the center-of-momentum frame ("isochronous" freeze–out). For one–dimensional (longitudinal) expansion the rapidity distributions are shown to differ significantly in the two scenarios, while the transverse momentum spectra are remarkably similar. We also investigate the rapidity distribution in greater detail and show that the Gaussian-like shape of this distribution commonly associated with the Landau expansion model in general emerges only if one neglects contributions from time-like parts of the isothermal freeze–out hypersurface.

[†]Supported by BMBF, DFG, GSI, and DOE.

[‡]Partially supported by the Alexander von Humboldt–Stiftung under the Feodor–Lynen program and by the Director, Office of Energy Research, Division of Nuclear Physics of the Office of High Energy and Nuclear Physics of the U.S. Department of Energy under Contract No. DE-FG-02-93ER-40764.

1 Introduction

Relativistic hydrodynamic models are frequently applied to study high–energy heavy–ion collisions [1, 2], because they simply represent (local) energy–momentum and charge conservation. Their main advantage is that they provide a *direct* link between space–time dynamics, i.e., observable flow phenomena, and the nuclear matter equation of state. They are therefore a unique tool to investigate e.g. effects of phase transitions, such as the deconfinement transition to the quark–gluon plasma, on the dynamics of the reaction [2, 3, 4, 5].

Relativistic hydrodynamics requires the assumption of *local thermodynamical equilibrium*[1], i.e., it describes the evolution of an *ideal* fluid [6]. This assumption obviously breaks down in the very early stages of ultrarelativistic heavy–ion collisions (the stopping power of nuclear matter is insufficient to produce immediate thermalization of matter in the collision zone) and in the very late stages of heavy–ion collisions at all energies. In this stage, the interaction rate between individual particles becomes too small, or equivalently, their mean free path between collisions becomes too long, to maintain local thermodynamical equilibrium in the expanding system, and non–equilibrium processes become dominant. Eventually, particles will decouple completely and stream freely until they reach the detector.

In order to calculate experimental observables it is essential to incorporate this so-called *freeze–out* into the hydrodynamical simulation of a heavy–ion collision. The long mean free path or the small interaction rate, respectively, suggest a treatment of the freeze–out via kinetic theory [7]. Up to now, however, no attempt has been made to combine the hydrodynamical and the kinetic description to model the late expansion stage of a heavy–ion collision. The most simple and therefore often used method is to assume an *instantaneous* transition from fluid-dynamical motion to free–streaming. Note that microscopic models for heavy–ion collisions [8] do not encounter this problem, since they follow the trajectories of individual particles. On the other hand, their disadvantage is that they do not provide a direct link to the nuclear matter equation of state and, when based on binary scatterings, become invalid for higher densities.

In this paper we present a systematic comparison of two different instantaneous freeze–out scenarios presently used in the literature, namely the freeze–out across a space–time hypersurface defined by a constant temperature (referred to as "isothermal" freeze–out in the following) and that across one defined by a constant time in the center-of-momentum (CM) frame of the system, respectively (subsequently termed "isochronous" freeze–out). Contributions from time-like and space-like parts of the hypersurface[2] are discussed separately and it is shown that the often used approximation of neglecting the time-like contributions in the isothermal freeze–out scenario leads to serious distortions of the rapidity spectra, and moreover violates the conservation laws.

The above freeze–out scenarios are not strictly self-consistent, because the hypersurface is determined *after* the fluid-dynamical problem has been solved in the *whole* forward light cone. In other words, the influence of the freeze–out of particles from the (time-like or

[1] A well-defined theory of relativistic dissipative hydrodynamics, which would allow for deviations from local thermodynamical equilibrium, does not yet exist, see for instance the discussion in [2].

[2] A definition of time-like and space-like surfaces is given in Section 3.

space-like) surface of the fluid on the dynamical evolution is neglected. Although attempts to treat this problem analytically have been made [9], up to now no generally accepted solution exists.

This paper is organized as follows. In Section 2 we present the underlying relativistic hydrodynamic expansion model. In Section 3 we introduce the two different freeze–out scenarios. Section 4 contains a discussion of single–inclusive rapidity distributions and transverse momentum spectra. In Section 5 we present our results and close with a summary in Section 6. We use natural units, $\hbar = k_B = c = 1$.

2 The expansion model

Since we want to focus on the effects of different freeze–out scenarios on the final particle spectra, we choose a particularly simple and transparent hydrodynamic expansion model, namely the one–dimensional expansion of a finite slab of matter with an ultrarelativistic ideal gas equation of state. This model was first studied by Landau et al. [10]. The expansion with Landau initial conditions can to first approximation serve to describe the evolution of (net) baryon–free matter in the central region of ultrarelativistic heavy–ion collisions ($\sqrt{s} \sim 100\,\mathrm{AGeV}$). In the following we briefly outline the essential ingredients and results of the Landau expansion model.

In general, relativistic hydrodynamics implies (local) energy–momentum conservation,

$$\partial_\mu T^{\mu\nu} = 0 \ , \tag{1}$$

where for an ideal fluid the energy–momentum tensor reads

$$T^{\mu\nu} = (\epsilon + p) u^\mu u^\nu - p g^{\mu\nu} \ . \tag{2}$$

Here, ϵ and p denote the energy density and pressure in the local rest frame of matter, $g^{\mu\nu} = \mathrm{diag}(+1, -1, -1, -1)$ is the metric tensor, and u^μ is the fluid 4–velocity ($u^\mu u_\mu = 1$). The system of eqs. (1, 2) is closed by choosing an equation of state for the matter under consideration. For an ultrarelativistic ideal gas this is

$$p = c_s^2 \, \epsilon \ , \tag{3}$$

with $c_s = 1/\sqrt{3}$ being the velocity of sound. For the particular application to heavy–ion collisions, we may think of an ideal (massless) pion gas. Then, the energy density is given in terms of the temperature T as

$$\epsilon = g \, \frac{\pi^2}{30} \, T^4 \ , \tag{4}$$

where $g = 3$ is the degeneracy factor for pions (assuming isospin symmetry). The particle density n in the local rest frame is

$$n = g \, \frac{\zeta(3)}{\pi^2} \, T^3 \ . \tag{5}$$

In the CM frame, the initial conditions for the one–dimensional expansion of a finite slab of length $2\,L$ into vacuum [10] are

$$\epsilon(0,z) = \begin{cases} \epsilon_0 & , \quad |z| \leq L \\ 0 & , \quad |z| > L \ , \end{cases} \tag{6}$$

$$v(0,z) = \begin{cases} -1 & , \quad -\infty < z < -L \\ 0 & , \quad -L \leq z \leq L \\ 1 & , \quad L < z < \infty \ . \end{cases} \tag{7}$$

Note that all lengths and times scale with L.

The system evolves as follows, cf. Fig. 1. Initially, the discontinuities at $z = \pm L$ decay into two simple (Riemann) rarefaction waves. The wave fronts move into the slab with velocities $\pm c_s$ and into the vacuum with the speed of light ± 1. At the CM time $t_m = L/c_s$ the two simple waves meet at the center and begin to overlap. At later times $t > t_m$ there are three distinct regions of hydrodynamic flow in the forward light cone. We call the one at the center of the system, where the two rarefaction waves overlap, the *Landau region* [10, 11, 12], because Landau was the first to determine the hydrodynamic solution in this region. The other two are called *Riemann regions*, because here the hydrodynamic solution is still given by the original simple Riemann rarefaction waves.

Since we ultimately want to apply the freeze–out scenarios discussed in this work to more complicated, three–dimensional simulations, we study the Landau expansion numerically. For the numerical solution we employ the explicit SHASTA algorithm [13]. The applicability of this version of SHASTA to relativistic one–dimensional compression and expansion problems in thermodynamically normal matter has been demonstrated in Refs. [14, 15]. We employ a reduced antidiffusion and also a simple full–step method for updating source terms[3].

The initial temperature profile and typical profiles for times $t > t_m$ are shown in Fig. 2. The temperature is calculated from the local energy density ϵ according to (4), and normalized to the initial temperature T_0. Note that the overlapping rarefaction waves in the Landau region produce a local minimum of energy density and temperature at fixed CM times $t > t_m$. This is essentially a relativistic effect: faster matter at larger $|z|$ experiences more time dilation and thus cools not as fast in the CM frame as slower matter near the center [14].

3 The freeze–out scenarios

3.1 General aspects

A particle "freezes out" when its interactions with the rest of the system cease. In principle, this can happen at any space–time point of the many–particle evolution, depending on the

[3]The half–step treatment of source terms is necessary only to appropriately describe compression shocks [14].

(finite) mean free path of the particular particle. In a one–component system, the mean free path is estimated as

$$\lambda \simeq \frac{1}{n\sigma} \ , \tag{8}$$

where σ is the (total) cross section and n the (local) comoving particle density. If λ is small enough such that local thermodynamical equilibrium is established, ideal hydrodynamics is valid (and n is, for a pionic system, given by eq. (5)). For larger λ non–equilibrium effects become increasingly important, and if λ exceeds the system's dimension D, the latter starts to decouple into free–streaming particles. To describe the system's evolution in the latter two stages in principle requires kinetic theory.

Up to now, drastic simplifications of the freeze–out stage were made for practical calculations [10, 16]. The first assumption is that the intermediate region where $\lambda \sim D$ has negligible extent and can be approximated by a hypersurface in space–time. When a fluid element crosses this hypersurface, particles contained in that element freeze out instantaneously. The second assumption is that the freeze–out of particles does not change the hydrodynamical evolution. Because of energy and momentum carried away by the leaving particles, the hydrodynamical solution is obviously influenced. Also, the decoupling of a particle from the flow perturbes (local) thermodynamic and chemical equilibrium in the respective fluid element. In general, the freeze–out should be treated in a self-consistent way taking all these effects into account. This, however, is out of the scope of the present work.

As mentioned in the Introduction, here we also assume instantaneous freeze–out across a hypersurface. We focus on two different scenarios. The first, referred to in the following as *isothermal freeze–out*, corresponds to freeze–out at a constant fluid temperature T_f. The second corresponds to freeze–out at a constant CM time t_f and is referred to as *isochronous freeze–out*.

3.2 Isothermal freeze–out

The isothermal freeze–out is based on assumptions originally formulated by Landau [10]. He argued that the freeze–out of an interacting hadronic fluid into free–streaming particles takes place at a certain freeze–out temperature T_f which, according to eq. (8) with $\lambda \sim D$, depends only weakly on the system's size, $T_f \sim D^{-1/3}$. Thus, the isotherm with $T = T_f$ defines the freeze–out hypersurface. For pions we have (roughly) $\sigma \sim 1$ fm^2 (at the energy scale relevant for pion–pion collisions in a thermal ensemble). We also assume $D \sim 2\,t_f \simeq 20\,L \sim 10$ fm (cf. Fig. 2), where the initial size of the hot central region was estimated to be $2\,L \sim 2\,t_0 \sim 1$ fm (for an equilibration time $t_0 \sim 0.5$ fm after impact), and obtain with eq. (5) the freeze–out criterion $T_f \simeq m_\pi$, where $m_\pi \simeq 138$ MeV is the pion mass.

In order to apply this scenario to our underlying expansion model presented in Section 2, the isotherm of temperature T_f has to be found numerically on the calculational grid. As an example, Fig. 1 shows the isotherm $T_f = 0.4\,T_0$. The isotherm is in very good agreement with that calculated with the (semi–analytical) method of characteristics, see [17].

A hypersurface element is called space-like if its normal vector is time-like, and vice versa. The whole isothermal hypersurface can be divided into space- and time-like parts according

to Fig. 1.

3.3 Isochronous freeze–out

Due to its simplicity, the isochronous freeze–out scenario is widely used in (3+1)–dimensional one– and multi–fluid-dynamics [1]. The freeze–out condition one commonly assumes is that the *average* temperature of the system at CM time t_f drops below a given value T_f,

$$\bar{T}(t_f) = T_f \ , \tag{9}$$

where $\bar{T}(t)$ is calculated according to

$$\bar{T}(t) = \frac{\int_{-L-t}^{L+t} \mathrm{d}z \, T\gamma n}{\int_{-L-t}^{L+t} \mathrm{d}z \, \gamma n} \ , \tag{10}$$

where $\gamma = (1-v^2)^{-1/2}$ and n is the local rest frame density given by eq. (5).

Note that the hypersurface for isochronous freeze–out is purely space-like. Fig. 1 shows the hypersurfaces at CM times t_f when (a) the *average* temperature is $\bar{T} = 0.4\, T_0$ ($t \simeq 9.2\,\mathrm{L}$, lower line), and (b) when the *maximum* temperature in the system has dropped below T_f ("late" isochronous freeze–out, $t \simeq 12.6\,\mathrm{L}$, upper line). Fig. 2 shows the corresponding temperature profiles.

Although the isochronous freeze–out surfaces are purely space-like, we distinguish "time-like" (dotted) and "space-like" (full line) parts as shown in Fig. 1. This is motivated by the situation at "late" isochronous freeze–out: the energy and momentum associated with particles freezing out across Σ_t in the isothermal freeze–out scenario later has to cross the dotted, "time-like" parts of the "late" isochronous freeze–out surface, because it cannot leave the forward light cone. On the other hand, the energy and momentum freezing out across Σ_s is the same that freezes out across the "space-like" part of the "late" isochronous freeze–out surface.

4 Calculation of the spectra

4.1 The Cooper–Frye formula

In both freeze–out scenarios, the distribution of particles that have decoupled from the fluid is determined as follows. The (Lorentz–invariant) momentum–space distribution of particles crossing a hypersurface Σ in Minkowski space is given by [16]

$$E\,\frac{\mathrm{d}N}{\mathrm{d}^3\mathbf{k}} = \int_\Sigma \mathrm{d}\sigma_\mu k^\mu \, f(k^\nu u_\nu) \ , \tag{11}$$

where $f(k^\nu u_\nu)$ is the local equilibrium distribution function

$$f(k^\nu u_\nu) = \frac{g}{(2\pi)^3} \frac{1}{\exp(k^\nu u_\nu/T) - 1} \ , \tag{12}$$

and $\mathrm{d}\sigma_\mu$ is the normal vector on an (infinitesimal) element of the hypersurface Σ. $\mathrm{d}\sigma_\mu$ is naturally chosen to point outwards with respect to the hotter interior of Σ, since (11) is supposed to give the momentum distribution of particles decoupling from the fluid. In our case of one–dimensional geometry, the transverse dimensions enter only as a (constant) transverse area factor A. The parametric integration over the hypersurface Σ in (11) is performed by distinguishing space-like parts Σ_s (with z as integration variable) and time-like parts Σ_t (with t as integration variable), cf. Fig. 1. This yields the total momentum–space distribution

$$\begin{aligned}\frac{\mathrm{d}N}{\mathrm{d}yk_\perp\mathrm{d}k_\perp} &= \frac{gA}{4\pi^2}\,m_\perp\left[\int_{\Sigma_s}\mathrm{d}z\;\frac{\sinh y(\partial t/\partial z)_\Sigma-\cosh y}{\exp\{m_\perp\cosh(\alpha-y)/T\}-1}\right.\\ &\left.+\int_{\Sigma_t}\mathrm{d}t\;\frac{\sinh y-\cosh y(\partial z/\partial t)_\Sigma}{\exp\{m_\perp\cosh(\alpha-y)/T\}-1}\right]\,, \qquad (13)\end{aligned}$$

where $y=\mathrm{Artanh}(k_\parallel/E)$ is the (longitudinal) particle rapidity, $m_\perp=(\mathbf{k}_\perp^2+m^2)^{1/2}$ is the transverse mass (which reduces to $k_\perp$ for massless particles), and $\alpha=\mathrm{Artanh}(v)$ is the (longitudinal) fluid rapidity. $(\partial t/\partial z)_\Sigma$ and $(\partial z/\partial t)_\Sigma$ are the (local) slope of the space-like and the inverse slope of the time-like hypersurface element, respectively. Note that the parametric integration in eq. (13) holds for a mathematically positive orientation of Σ.

4.2 Application to isothermal freeze–out

We now apply eq. (13) to the isothermal freeze–out scenario. Along the isotherm, $T=T_f=$ const. and only α depends on position or time, respectively. The rapidity distribution is obtained by integrating (13) over transverse momentum. For massless particles,

$$\begin{aligned}\frac{1}{AT_0{}^3}\frac{\mathrm{d}N}{\mathrm{d}y} &= \frac{g\zeta(3)}{2\pi^2}\left(\frac{T_f}{T_0}\right)^3\left[\int_{\Sigma_s}\mathrm{d}z\;\frac{\sinh y(\partial t/\partial z)_\Sigma-\cosh y}{\cosh^3(\alpha(z)-y)}\right.\\ &\left.+\int_{\Sigma_t}\mathrm{d}t\;\frac{\sinh y-\cosh y(\partial z/\partial t)_\Sigma}{\cosh^3(\alpha(t)-y)}\right]\,. \qquad (14)\end{aligned}$$

Analogously, the transverse momentum distribution is obtained integrating over y,

$$\begin{aligned}\frac{1}{AT_0}\frac{\mathrm{d}N}{k_\perp\mathrm{d}k_\perp} &= \frac{g}{4\pi^2}\,\frac{k_\perp}{T_0}\left[\int_{\Sigma_s}\mathrm{d}z\;\int_{-\infty}^{\infty}\mathrm{d}y\;\frac{\sinh y(\partial t/\partial z)_\Sigma-\cosh y}{\exp\{(k_\perp/T_0)(T_0/T_f)\cosh(\alpha(z)-y)\}-1}\right.\\ &\left.+\int_{\Sigma_t}\mathrm{d}t\;\int_{-\infty}^{\infty}\mathrm{d}y\;\frac{\sinh y-\cosh y(\partial z/\partial t)_\Sigma}{\exp\{(k_\perp/T_0)(T_0/T_f)\cosh(\alpha(t)-y)\}-1}\right]\,. \qquad (15)\end{aligned}$$

4.3 Application to isochronous freeze–out

In the isochronous freeze–out scenario the hypersurface Σ has no time-like part and the second term in (13) vanishes. Moreover, also the first term in the numerator of the remaining

term vanishes due to $\partial t/\partial z = 0$ for this particular hypersurface. The temperature along the hypersurface, however, is no longer constant. Thus the rapidity distribution becomes

$$\frac{1}{AT_0^3}\frac{\mathrm{d}N}{\mathrm{d}y} = \frac{g\zeta(3)}{2\pi^2}\int_{-L-t_f}^{L+t_f}\mathrm{d}z\left(\frac{T(z)}{T_0}\right)^3\frac{\cosh y}{\cosh^3(\alpha(z)-y)}\ , \tag{16}$$

while the transverse momentum distribution is

$$\frac{1}{AT_0}\frac{\mathrm{d}N}{k_\perp \mathrm{d}k_\perp} = \frac{g}{4\pi^2}\,\frac{k_\perp}{T_0}\int_{-L-t_f}^{L+t_f}\mathrm{d}z\int_{-\infty}^{\infty}\mathrm{d}y\,\frac{\cosh y}{\exp\{(k_\perp/T_0)(T_0/T(z))\cosh(\alpha(z)-y)\}-1}\ . \tag{17}$$

Note that the boundaries of the z–integration correspond to the light cone.

5 Results

In this section we discuss the pion rapidity and transverse momentum spectra for isothermal and isochronous freeze–out using the expansion model of Section 2. Note that for ideal fluid dynamics, entropy is conserved. Since for a gas of massless particles the particle number density is proportional to the entropy density, $n = 45\,\zeta(3)s/2\,\pi^4$, also the total particle number is conserved. The rapidity distributions presented in this section are numerically checked to fulfill this conservation law to better than 2% accuracy (across hypersurfaces bounded by the light cone).

In Fig. 3 we present the rapidity spectrum for isothermal freeze–out, eq. (14), along the isotherm $T_f = 0.4\,T_0$ that was shown in Fig. 1. The contributions from the different parts of the hypersurface as indicated in Fig. 1 are shown separately. The total spectrum (full line) shows a double–peak structure, and a small local maximum at $y = 0$. The time-like contributions (dashed) can become negative for particles with a longitudinal velocity $\tanh y$ which is smaller than the inverse slope of the time-like hypersurface, because then $\sinh y - \cosh y(\partial z/\partial t)_\Sigma = \cosh y[\tanh y - (\partial z/\partial t)_\Sigma] < 0$. These contributions correspond to particles that are overtaken by the freeze–out condition, and thus in principle re-enter the fluid instead of freezing out. Note that it is important to count these particles with their correct (negative) sign in order to ensure energy–momentum, entropy, and particle number conservation. As can be seen in Fig. 3, the space-like contributions to the spectrum (dash-dotted) are always positive, due to $|(\partial t/\partial z)_\Sigma| < 1$.

The transverse momentum spectrum, eq. (15), is shown in Fig. 4. Here one observes that the time-like part of the hypersurface (dashed) contributes less particles than the space-like one (dash-dotted), but the slope is the same, reflecting the fact that the temperature along the isothermal freeze–out hypersurface is constant by definition. The observed low–$k_\perp$ enhancement is due to Bose–Einstein statistics.

For comparison, Fig. 5 shows the rapidity spectrum for isochronous freeze–out, eq. (16), with $\bar{T} = 0.4\,T_0$. The total spectrum (full line) shows a double–peak structure with a local minimum at $y = 0$ which originates from the time dilation effect discussed in Section 2. Different contributions from the "time-like" and "space-like" parts as defined in Section 3.3

are shown separately (dashed, dash-dotted lines). As is obvious from eq. (16), there are no negative contributions to the spectrum.

The corresponding transverse momentum spectrum, eq. (17), is presented in Fig. 6. The "space-like" part of the fluid distribution has on the average a higher temperature and thus its contribution to the transverse momentum spectrum a smaller (negative) slope than the corresponding spectrum from the "time-like" parts. The total spectrum (full line) is nevertheless very similar to the one in the isothermal freeze–out, Fig. 4, because the *average* temperature at freeze–out is the same in both scenarios.

We now study the dependence of the spectra on the freeze–out temperature. Fig. 7 shows rapidity spectra for isothermal freeze–out at $T_f = 0.8,\ 0.6,\ 0.4,\ 0.2\,T_0$. For the largest T_f–values the rapidity spectrum peaks at finite y while for smaller T_f also a peak at central rapidity $y = 0$ develops. Only for $T_f \ll T_0$ does this peak dominate the spectrum.

In the case of isochronous freeze–out the situation is quite different. In Fig. 8, we show results for $\bar{T} = 0.8,\ 0.6,\ 0.4,\ 0.2\,T_0$. For $\bar{T} = 0.8\,T_0$, one observes a rapidity distribution with a Gaussian-like shape, because in this case freeze–out happens so early that the two maxima and the minimum at the origin as seen in the temperature distribution (Fig. 2) are too close together to be resolved after thermal smearing (especially since in this case the temperature is relatively high). Also, for decreasing freeze–out temperatures there are considerable differences to the case of isothermal freeze–out. In particular, there is no maximum at central rapidity due to the time dilation effect visible in the temperature distributions.

We now consider the variation of the transverse momentum spectrum with temperature. In Fig. 9 we present the different transverse momentum spectra for isothermal freeze–out and for the same freeze–out temperatures as above. As expected, lower freeze–out temperatures lead to steeper distributions. The corresponding spectra for isochronous freeze–out are shown in Fig. 10. Due to the above mentioned reasons, the results are very similar to those of isothermal freeze–out.

A Gaussian-like shape of the rapidity spectra is often claimed to be a characteristic feature of the Landau expansion model [10, 12]. As is demonstrated in Fig. 7, this is not true in general and especially not for realistic values of T_f. A Gaussian-like spectrum emerges *only* if one neglects the time-like contributions to the rapidity spectrum, which, however, dominate the sum spectra at higher T_f. To illustrate this point we show in Fig. 11 the rapidity spectrum originating from the space-like parts of the isothermal freeze–out hypersurface. Note that in contrast to Fig. 7, *all rapidity spectra have Gaussian-like shapes*. The neglected time-like contributions are shown separately in Fig. 12. We have normalized the spectra in Fig. 11 to their maximum value at $y = 0$ in order to facilitate a comparison to the results of Srivastava et al. [12] who employ this approximation. Note also that their method to calculate the spectra violates the conservation laws, since it does not account for energy, momentum, entropy, or particle number streaming through the time-like parts of the freeze–out hypersurface.

6 Summary and Conclusions

In this paper we have investigated freeze–out in a one–dimensional hydrodynamic model for the expansion stage of heavy–ion collisions. We have discussed two different freeze–out scenarios used in the literature, namely instantaneous freeze–out across an isothermal and an isochronous space–time hypersurface.

We have found that, provided $\bar{T}|_{t_f} = T_f$, the transverse momentum spectra are very similar in the two scenarios, but that there are noticeable differences in the rapidity distributions. This can be explained as follows. In our model, the fluid evolution is only one–dimensional and variations in temperature and fluid velocity occur only along the longitudinal direction. It is obvious that they consequently have to vary along different hypersurfaces in space–time. These differences are bound to reflect themselves in the (longitudinal) rapidity distribution. On the other hand, the transverse momentum spectra average over the longitudinal degrees of freedom and thus are only influenced by the (average) temperature. The fact that the latter is the same in both scenarios naturally explains the observed similarity. If one, however, selects a particular rapidity interval for the calculation of the transverse momentum spectra, for instance midrapidity, the main contribution will come from the space-like parts of the hypersurface at z=0, where the fluid temperature is different in the two scenarios, cf. Fig. 1. The transverse momentum spectra will reflect this difference, cf. Figs. 4 and 6. Therefore, one should in general use the (more realistic) isothermal freeze–out scenario in three–dimensional calculations. For central collisions with cylindrical symmetry, isothermal freeze–out was already employed in the calculations of Ref. [18].

We also demonstrated that an improper calculation of the particle rapidity distribution, neglecting contributions from time-like parts of the freeze–out hypersurface and thus violating the conservation laws, leads to the well–known Gaussian-like shapes commonly associated with the Landau expansion model. A consistent calculation, however, produces double– or triple–humped distributions.

Future studies should on the one hand focus on a more realistic description of the decoupling of particles from regions with finite space–time extent instead across an infinitely narrow space–time hypersurface. On the other hand, the feedback of the decoupling process on the evolution of the fluid has to be taken into account to obtain a fully self-consistent picture of freeze–out for the hydrodynamical description of heavy–ion collisions.

Acknowledgements

We thank Adrian Dumitru and Miklos Gyulassy for fruitful and enlightening discussions, and Adrian Dumitru for a careful reading of the manuscript. J.A.M. thanks the Nuclear Theory Group at Columbia University for its hospitality, where part of this work was done.

References

[1] see e.g.:
J.A. Maruhn, W. Greiner, in: 'Treatise on Heavy–Ion Science", Vol. 4 (ed. D.A. Bromley,

Plenum Press, New York, London, 1985), p. 565,
H. Stöcker and W. Greiner, Phys. Rep. 137 (1986) 277,
K. Kajantie, M. Kataja, L. McLerran, and P.V. Ruuskanen, Phys. Rev. D 34 (1986) 2746,
E.F. Staubo, A.K. Holme, L.P. Csernai, M. Gong, D. Strottman, Phys. Lett. B 229 (1989), 351,
I.N. Mishustin, V.N. Russkikh, L.M. Satarov, Nucl. Phys. A 494 (1989) 595,
K.S. Lee, U. Heinz, E. Schnedermann, Z. Phys. C 48 (1990) 525,
B. Waldhauser et al., Z. Phys. C 54 (1992) 459,
U. Katscher et al., Prog. Part. Nucl. Phys. 30 (1993) 303,
U. Katscher, D.H. Rischke, J.A. Maruhn, W. Greiner, I.N. Mishustin, L.M. Satarov, Z. Phys. A 346 (1993) 209.

[2] R.B. Clare, D.D. Strottman, Phys. Rep. 141 (1986) 177,
D. Strottman, Nucl. Phys. A 566 (1994) 245c.

[3] L.V. Bravina, N.S. Amelin, L.P. Csernai, P. Levai, D. Strottman, Nucl. Phys. A 566 (1994) 461c.

[4] D.H. Rischke, Y. Pürsün, J.A. Maruhn, H. Stöcker, W. Greiner, Columbia University preprint CU–TP–695, nucl-th/9505014, to be published in Heavy Ion Phys.

[5] D.H. Rischke, M. Gyulassy, Columbia University preprint CU–TP–706, nucl-th/9509040, to be published in Nucl. Phys. A.

[6] L.D. Landau, E.M. Lifshitz, "Fluid mechanics" (Pergamon, New York, 1959).

[7] L.D. Landau, E.M. Lifshitz, "Physical Kinetics" (Pergamon, New York, 1959).

[8] see e.g.:
J. Aichelin, A. Rosenhauer, G. Peilert, H. Stöcker, W. Greiner, Phys. Rev. Lett. 58 (1987) 1926,
H. Sorge, H. Stöcker, W. Greiner, Ann. Phys. 192 (1989) 266.

[9] Y.M. Sinyukov, Z. Phys. C 43 (1989) 401,
M.I. Gorenstein, M.S. Tsai, S.N. Yang, Ukr.Acad.Sci., Bogolyubov Institute preprint ITP-94-04E.

[10] L.D. Landau, Izv. Akd. Nauk SSSR 17 (1953) 51, in: "Collected papers of L.D. Landau" (ed. D. Ter–Haar, Pergamon, Oxford, 1965), p. 569–585,
L.D. Landau, S.Z. Belenkii, Uspekhi Fiz. Nauk 56 (1955) 309, ibid., p. 665–700.

[11] T. Achenbach et.al., GSI scientific report (1991).

[12] D.K. Srivastava, J. Alam, S. Chakrabarty, B. Sinha, and S. Raha, Ann. of Phys. 228 (1993) 104.

[13] J.P. Boris, D.L. Book, J. Comput. Phys. 11 (1973) 38,
D.L. Book, J.P. Boris, K. Hain, J. Comput. Phys. 18 (1975) 248.

[14] D.H. Rischke, S. Bernard, J.A. Maruhn, Columbia University preprint CU–TP–692, nucl-th/9504018, to be published in Nucl. Phys. A.

[15] V. Schneider et al., J. Comput. Phys. 105 (1993) 92.

[16] F. Cooper, G. Frye, Phys. Rev. D 10 (1974) 186,
F. Cooper, G. Frye, E. Schonberg, Phys. Rev. D 11 (1975) 192.

[17] G. Baym, B.L. Friman, J.P. Blaizot, M. Soyeur, W. Czyż, Nucl. Phys. A 407 (1983) 541.

[18] U. Ornik, F.W. Pottag, and R.M. Weiner, Phys. Rev. Lett. 63 (1989) 2641,
B.R. Schlei, U. Ornik, M. Plümer, D. Strottman, R.M. Weiner, preprint LAUR-95-3232, hep-ph/9509426.

Figure Captions:

Fig. 1: Illustration of the different freeze–out scenarios. The expansion has been calculated with the explicit SHASTA. As an example for the isothermal freeze–out, we show the isotherm $T_f = 0.4\,T_0$. It consists of two parts, namely the time-like Σ_t (dashed), and the space-like Σ_s (dash-dotted). For the isochronous freeze–out, we show the (purely space-like) surfaces at the CM times when (a) the average temperature $\bar{T} = 0.4\,T_0$ is reached (lower line), and (b) the temperature of the hottest cell has just dropped below T_f ("late" freeze–out, upper line). Also for the isochronous scenario we define so-called "time-like" (dotted) and "space-like" (full) contributions, for an explanation see text. The thin dashed lines illustrate the boundaries between the Riemann and the Landau region.

Fig. 2: Temperature profiles for the one-dimensional expansion, normalized to the initial temperature T_0. Full line: initial profile. Also shown are profiles at (a) $t \simeq 9.2\,\mathrm{L}$, when the average temperature of the distribution is $\bar{T} = 0.4\,T_0$ (dashed), and (b) at $t \simeq 12.6\,\mathrm{L}$, when the late freeze–out stage is reached (dash-dotted). The profiles have been calculated with the explicit SHASTA and standard antidiffusion [14].

Fig. 3: Rapidity distribution (full line) for isothermal freeze–out along the isotherm $T_f = 0.4\,T_0$. The distribution consists of contributions from time-like (dashed) and space-like (dash-dotted) parts of the hypersurface. $V_0 = 2LA$ is the initial volume of the expanding block.

Fig. 4: Transverse momentum spectrum for isothermal freeze–out at $T_f = 0.4\,T_0$. Time-like (dashed) and space-like (dash-dotted) contributions are shown separately.

Fig. 5: Rapidity distribution (full line) for isochronous freeze–out with $\bar{T} = 0.4\,T_0$. The distribution consists of contributions from the "time-like" (dashed) and "space-like" (dash-dotted) parts of the hypersurface.

Fig. 6: Transverse momentum spectrum for isochronous freeze–out with $\bar{T} = 0.4\,T_0$. "Time-like" (dashed) and "space-like" (dash-dotted) contributions are shown separately.

Fig. 7: Rapidity distributions for isothermal freeze–out along the isotherms $T_f/T_0 =$ 0.8, 0.6, 0.4, 0.2. Only the total distributions are shown.

Fig. 8: Rapidity distributions for isochronous freeze–out at average temperatures $\bar{T}/T_0 =$ 0.8, 0.6, 0.4, 0.2. Only the total distributions are shown.

Fig. 9: Transverse momentum spectra for isothermal freeze–out along the isotherms $T_f/T_0 =$ 0.8, 0.6, 0.4, 0.2. Only the total spectra are shown.

Fig. 10: Transverse momentum spectra for isochronous freeze–out at average tempera-

tures $\bar{T}/T_0 = 0.8$, 0.6, 0.4, 0.2. Only the total spectra are shown.

Fig. 11: Rapidity distributions along the space-like part of the hypersurfaces for isothermal freeze–out with temperatures $T_f/T_0 = 0.8$, 0.6, 0.4, 0.2. The distributions have been normalized to their maximum value. The time-like parts of the hypersurfaces are neglected.

Fig. 12: The time-like contributions that have been neglected in Fig. 11. The distributions are normalized to the corresponding maxima in Fig. 11.

fig.01

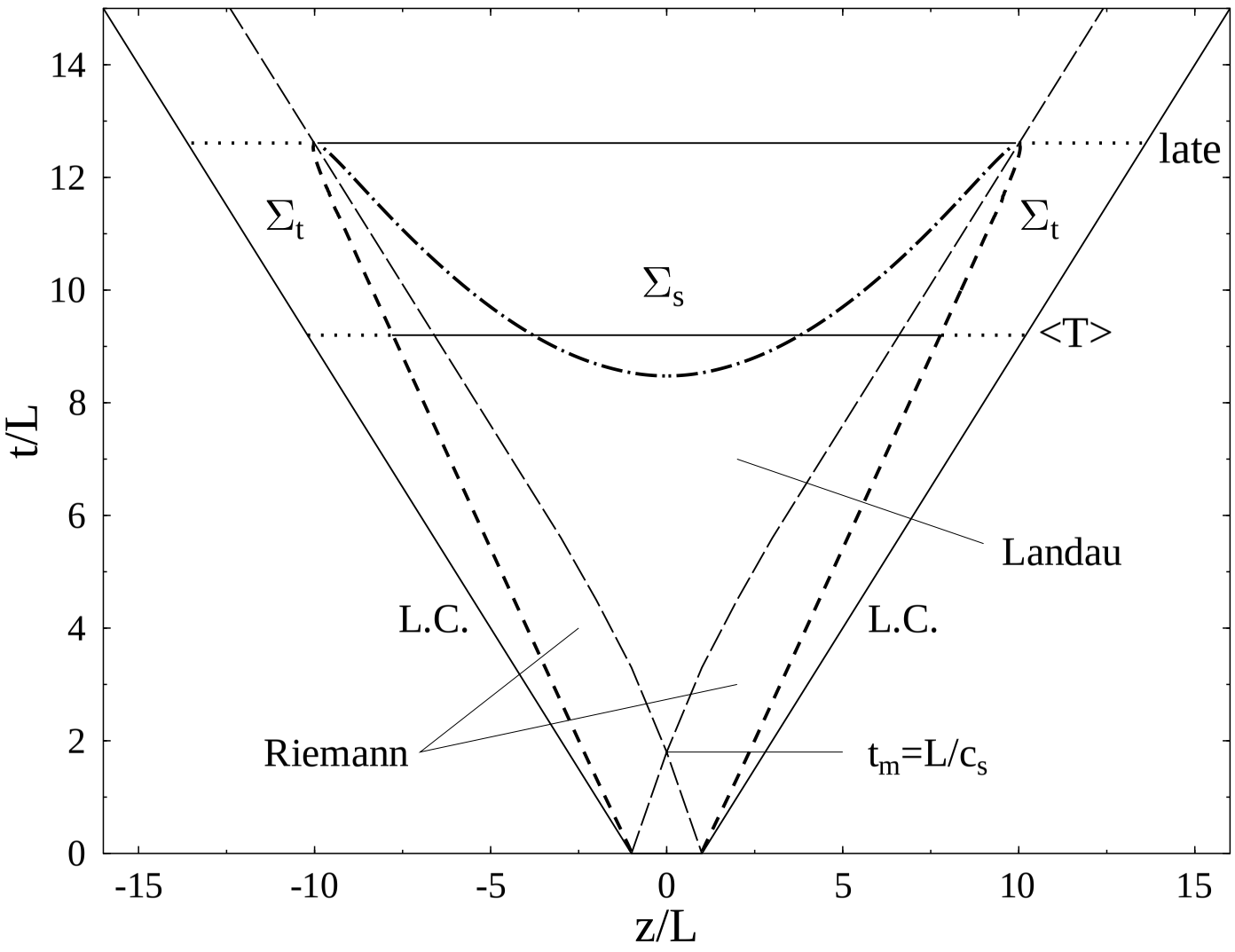
14
12
10
8
6
4
2
0
t/L
-15
-10
-5
0
5
10
15
z/L
late
Σ_t
Σ_t
Σ_s
<T>
Landau
L.C.
L.C.
Riemann
$t_m=L/c_s$

fig.02

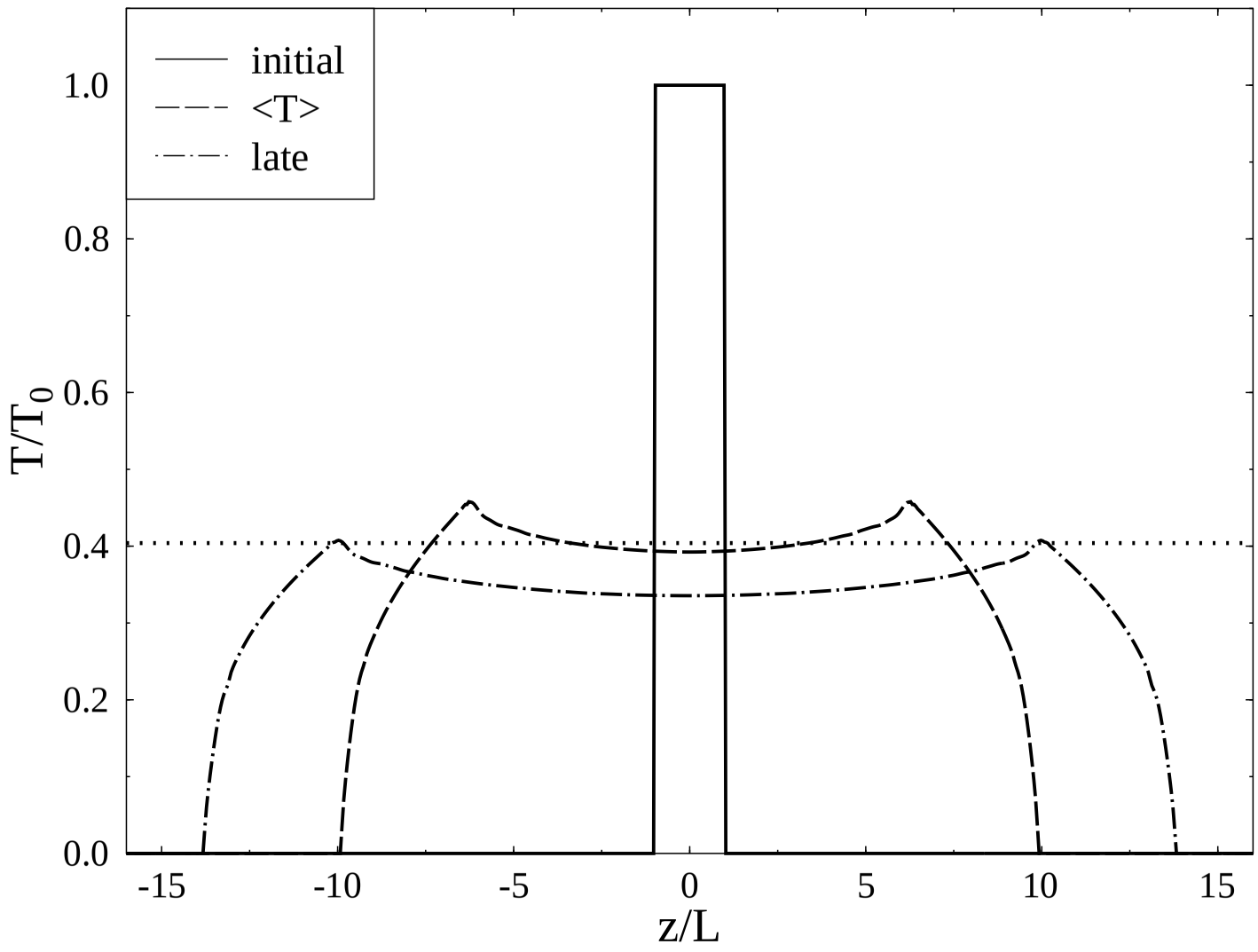

fig.03

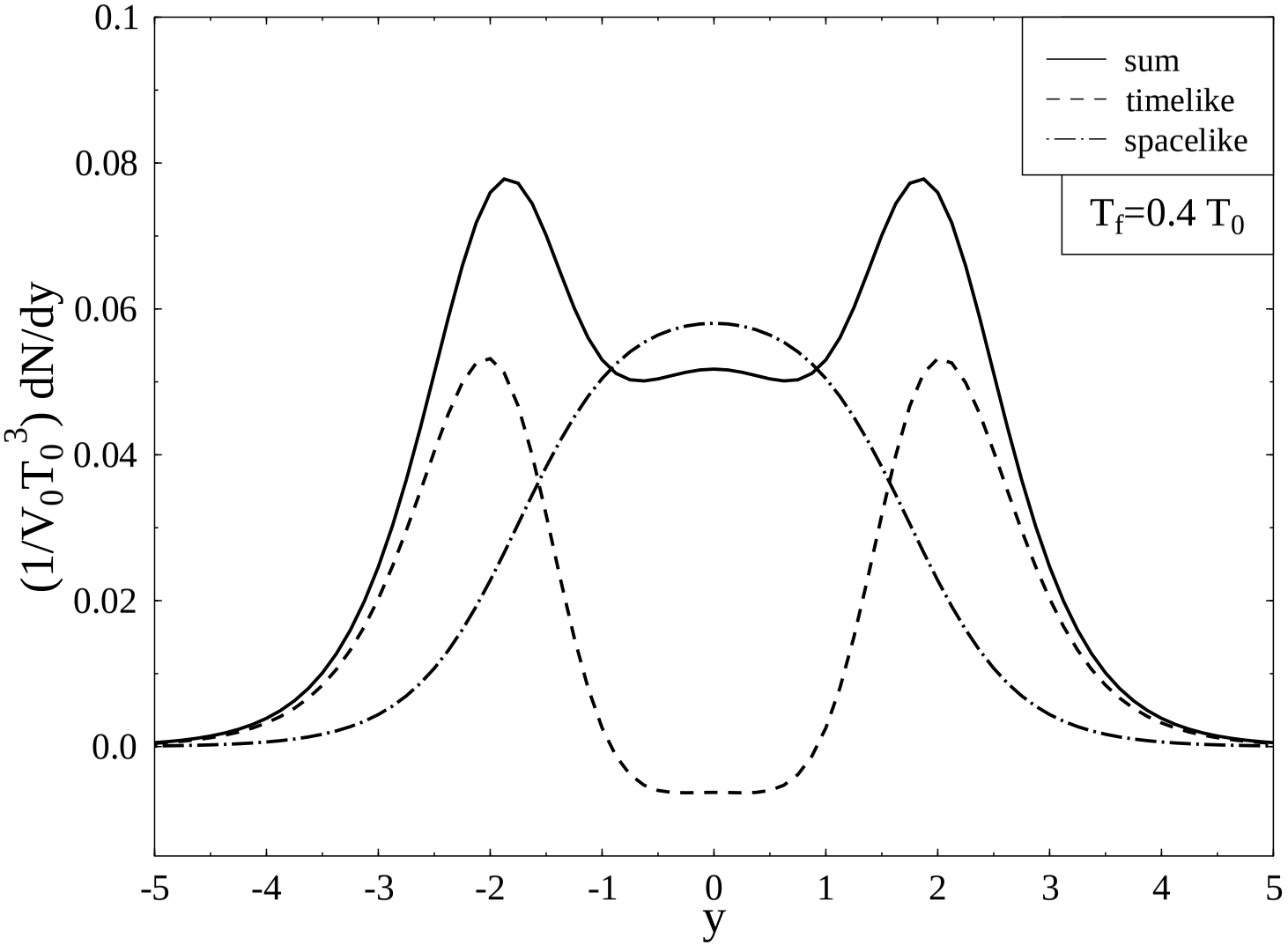
0.1
0.08
0.06
0.04
0.02
0.0
-5
-4
-3
-2
-1
0
1
2
3
4
5
y
(1/V0T0 3) dN/dy
sum
timelike
spacelike
Tf=0.4 T0

fig.04

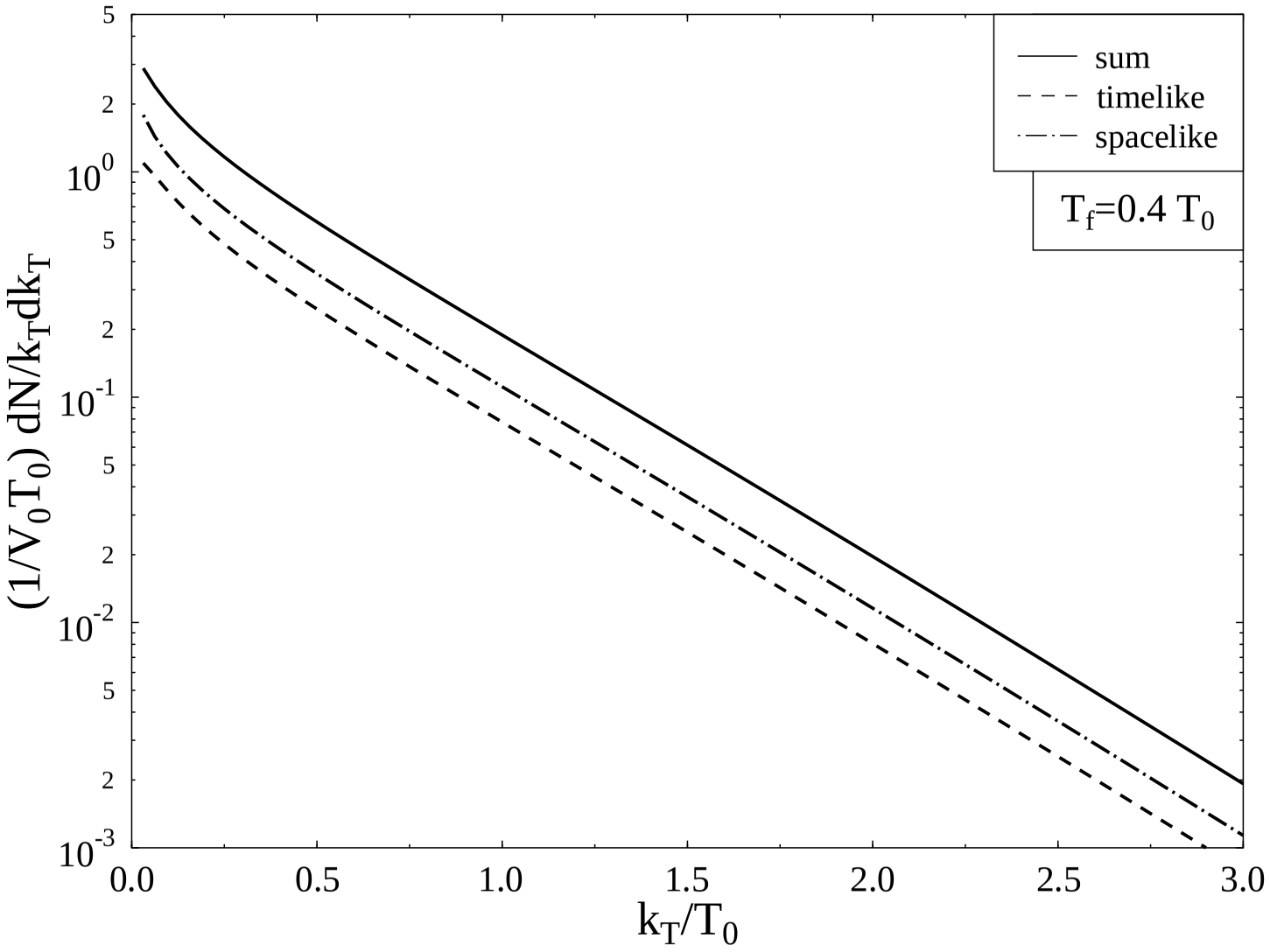
sum
timelike
spacelike
T_f=0.4 T_0
$(1/V_0T_0)\ dN/k_T dk_T$
k_T/T_0
0.0
0.5
1.0
1.5
2.0
2.5
3.0
10^{0}
10^{-1}
10^{-2}
10^{-3}

fig.05

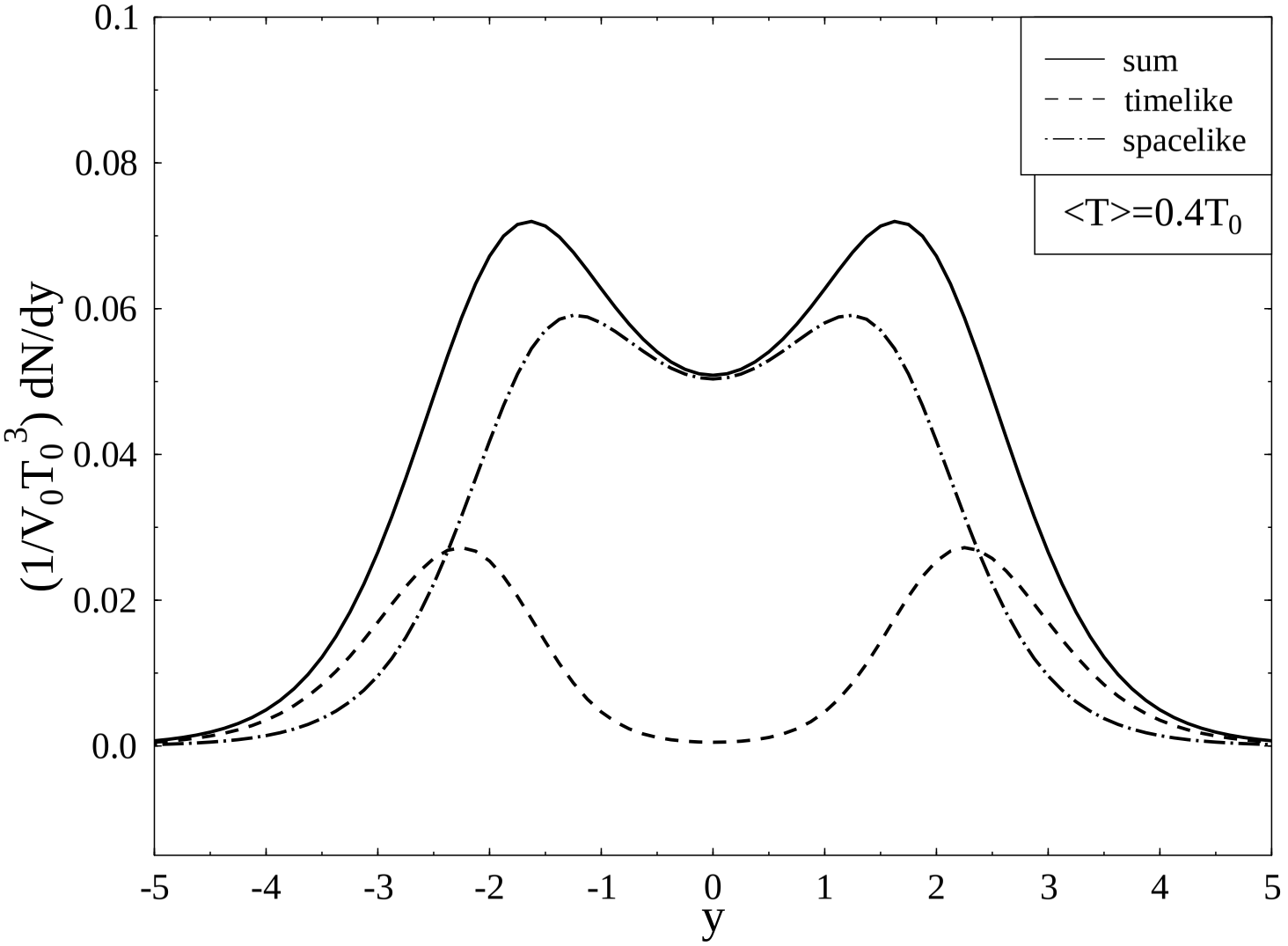
sum
timelike
spacelike
<T>=0.4T0
(1/V0T0 3) dN/dy
y
0.1
0.08
0.06
0.04
0.02
0.0
-5
-4
-3
-2
-1
0
1
2
3
4
5

fig.06

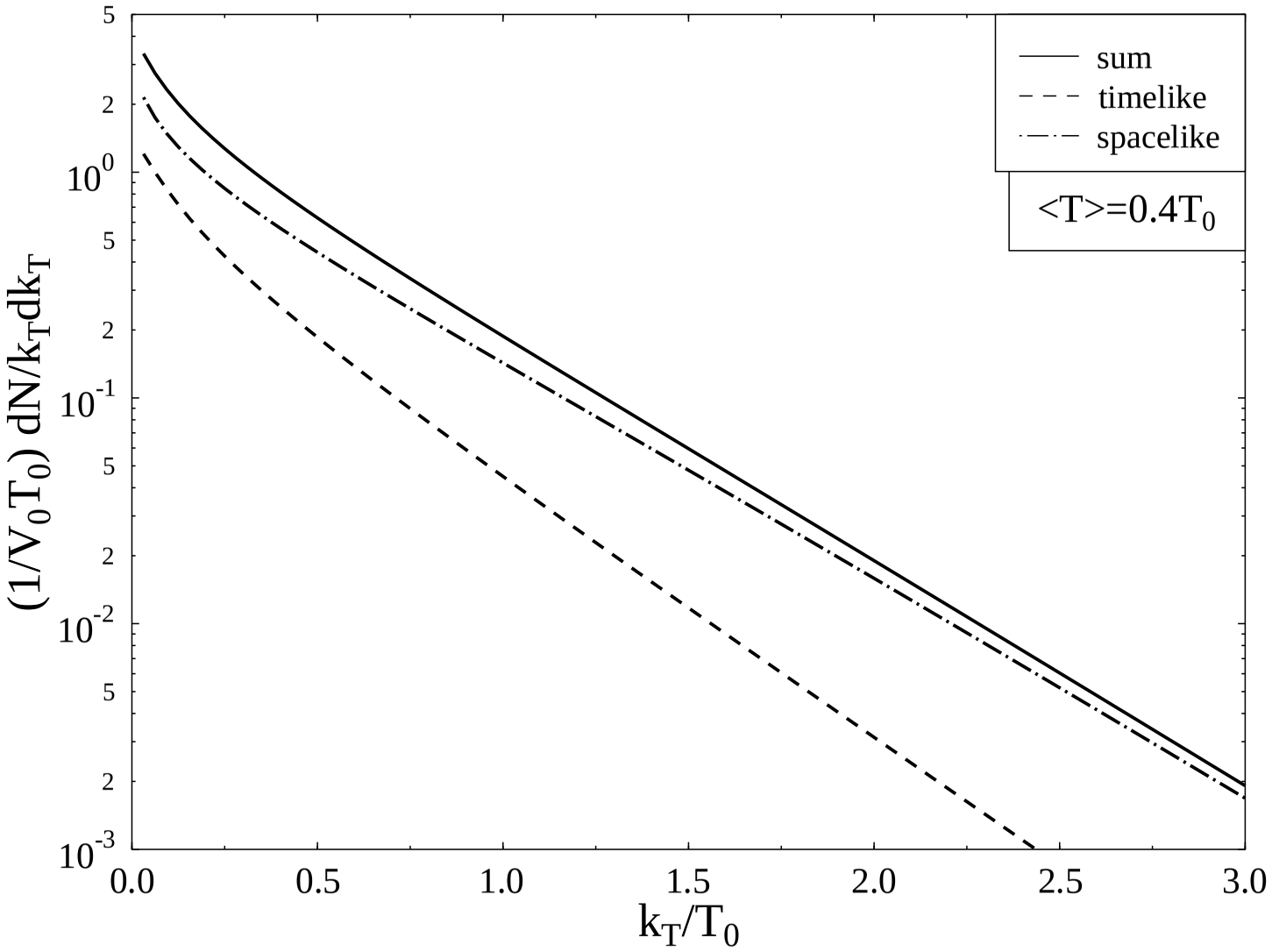
sum
timelike
spacelike
<T>=0.4T0
(1/V0T0) dN/kTdkT
kT/T0
5
2
10^0
5
2
10^-1
5
2
10^-2
5
2
10^-3
0.0
0.5
1.0
1.5
2.0
2.5
3.0

fig.07

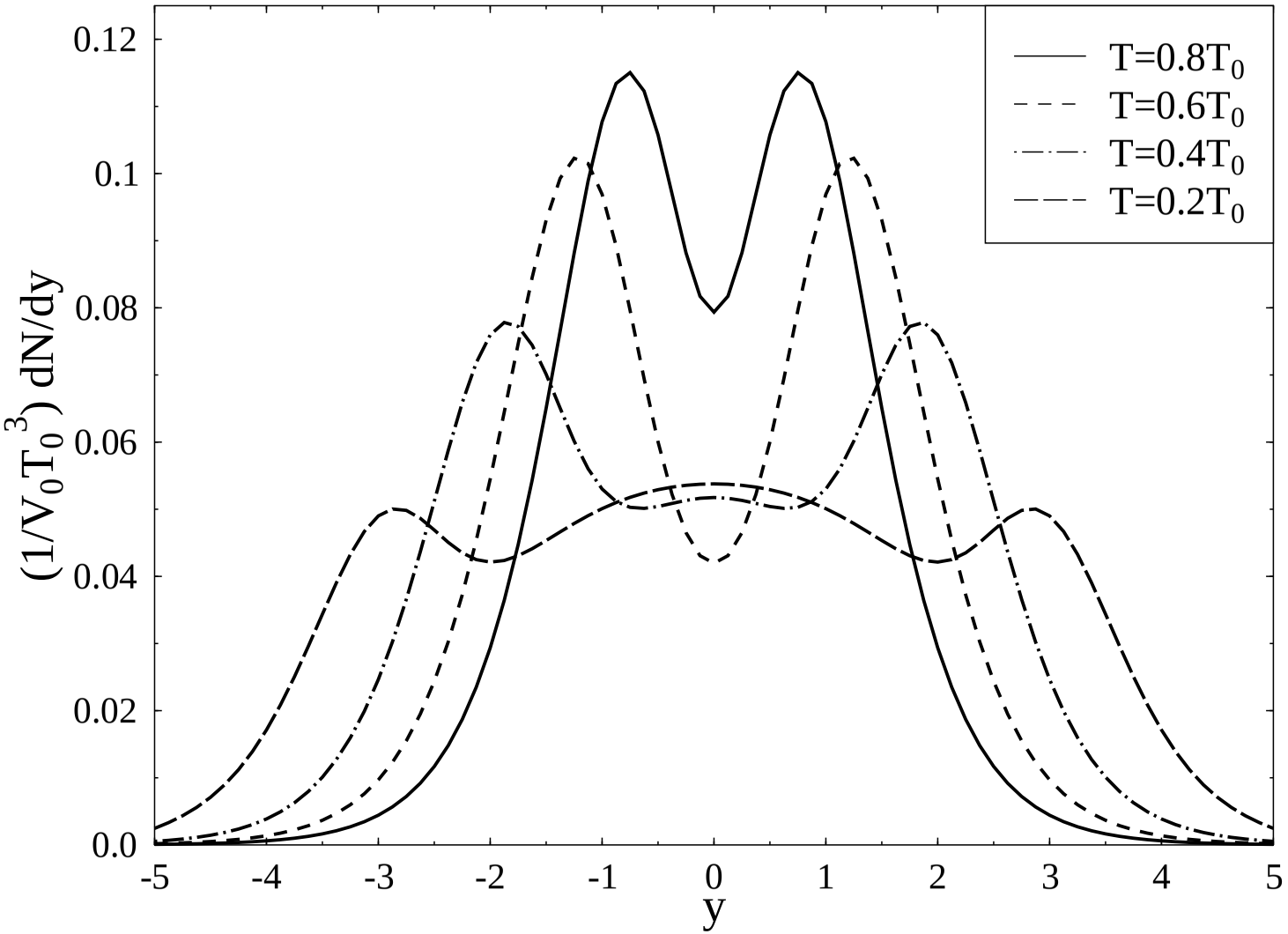
0.12
0.1
0.08
0.06
0.04
0.02
0.0
-5
-4
-3
-2
-1
0
1
2
3
4
5
y
(1/V0T0 3) dN/dy
T=0.8T0
T=0.6T0
T=0.4T0
T=0.2T0

fig.08

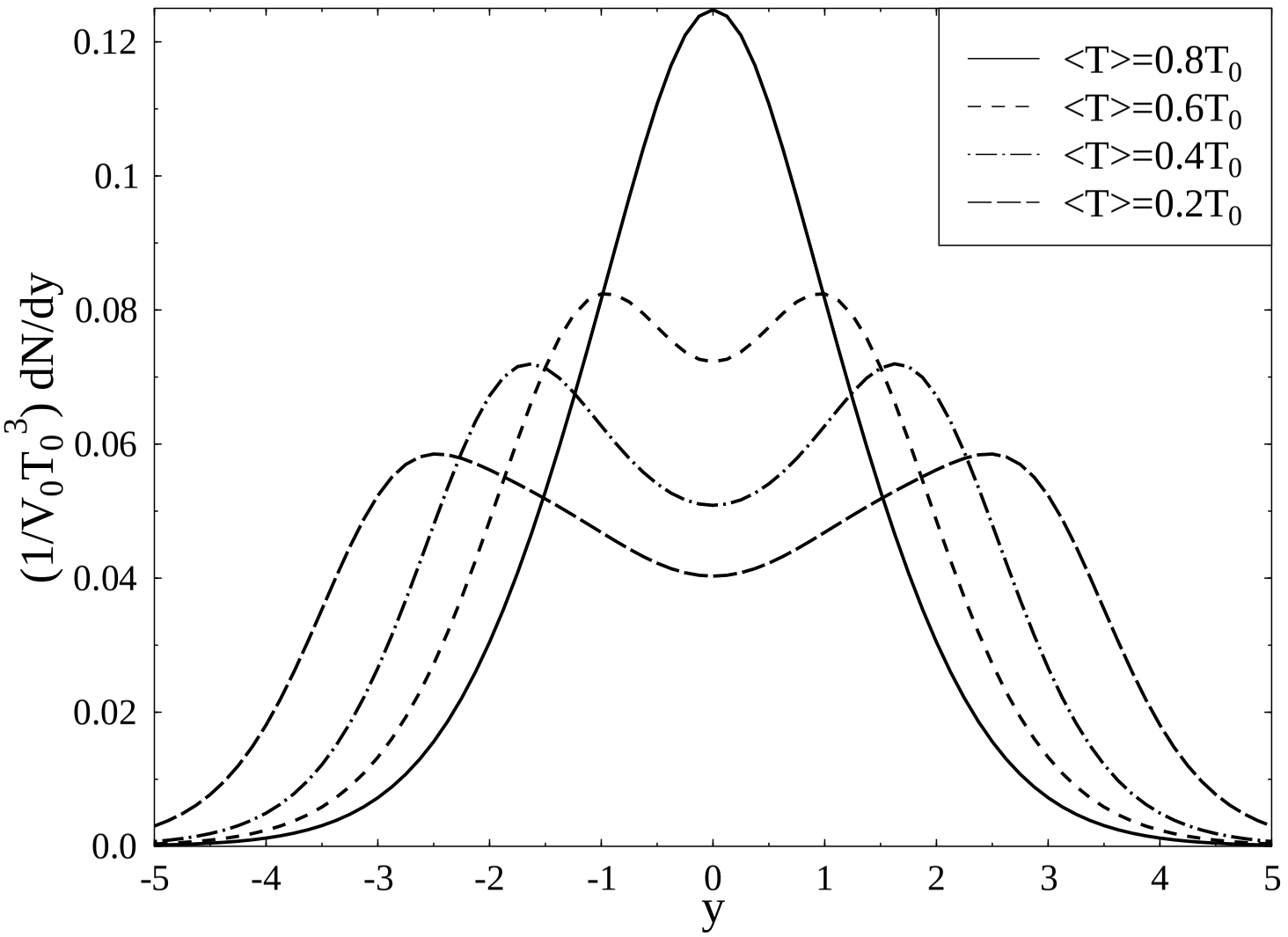
0.12
0.1
0.08
0.06
0.04
0.02
0.0
-5
-4
-3
-2
-1
0
1
2
3
4
5
y
(1/V0T0 3) dN/dy
<T>=0.8T0
<T>=0.6T0
<T>=0.4T0
<T>=0.2T0

fig.09

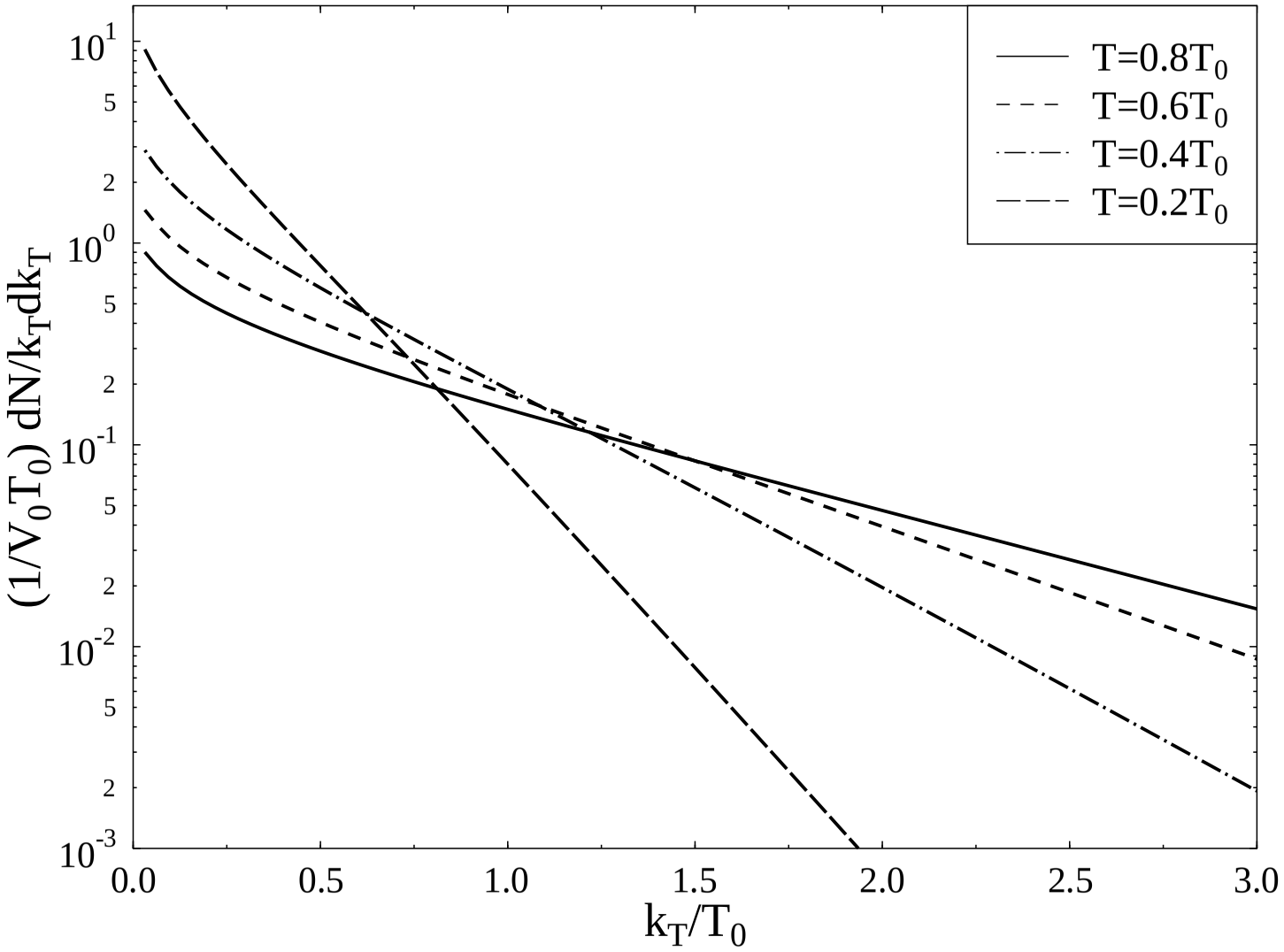
T=0.8T0
T=0.6T0
T=0.4T0
T=0.2T0
(1/V0T0) dN/kTdkT
kT/T0
10^1
5
2
10^0
5
2
10^-1
5
2
10^-2
5
2
10^-3
0.0
0.5
1.0
1.5
2.0
2.5
3.0

fig.10

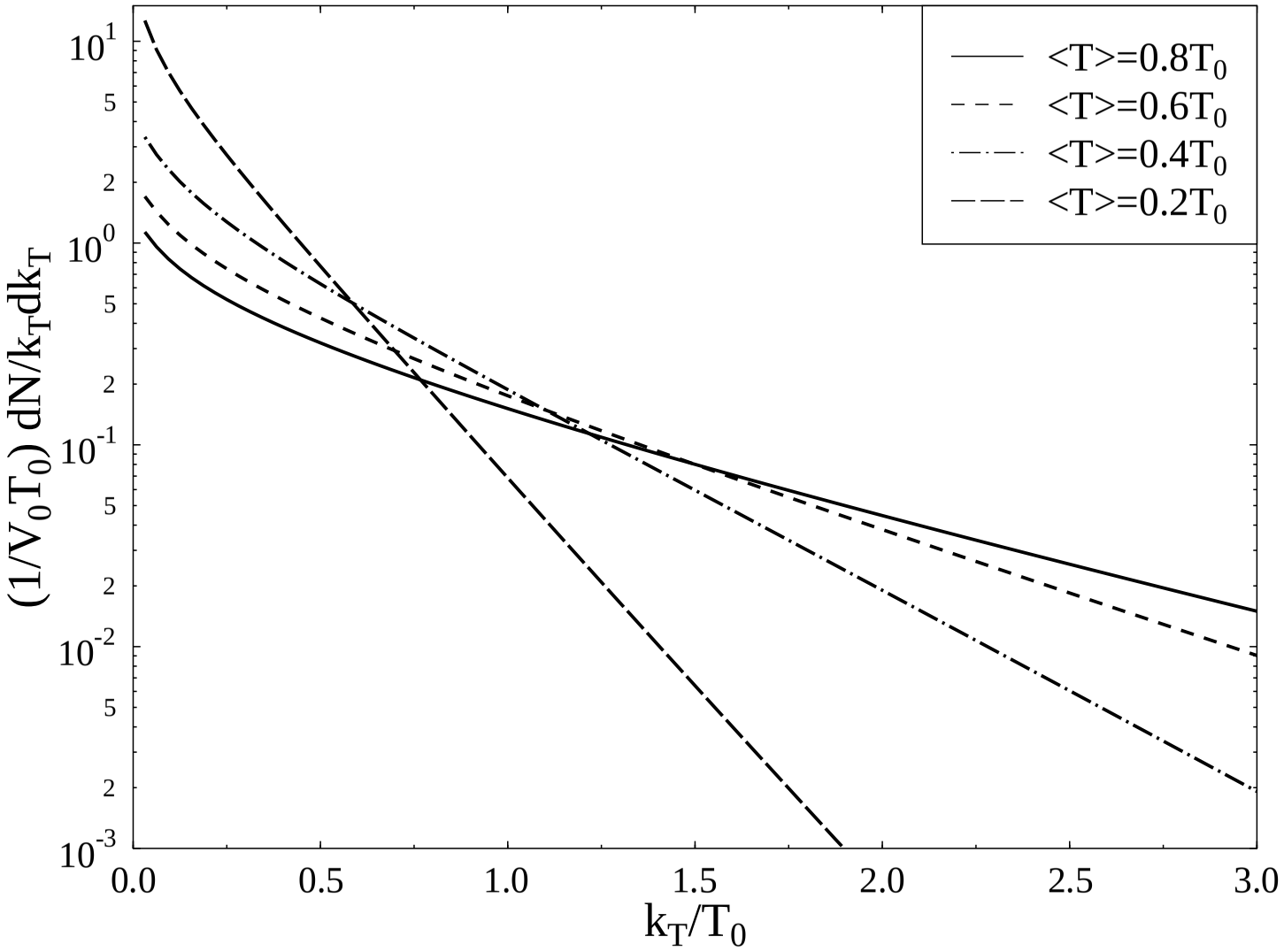
<T>=0.8T0
<T>=0.6T0
<T>=0.4T0
<T>=0.2T0
(1/V0T0) dN/kTdkT
kT/T0
10^1
5
2
10^0
5
2
10^-1
5
2
10^-2
5
2
10^-3
0.0
0.5
1.0
1.5
2.0
2.5
3.0

fig.11

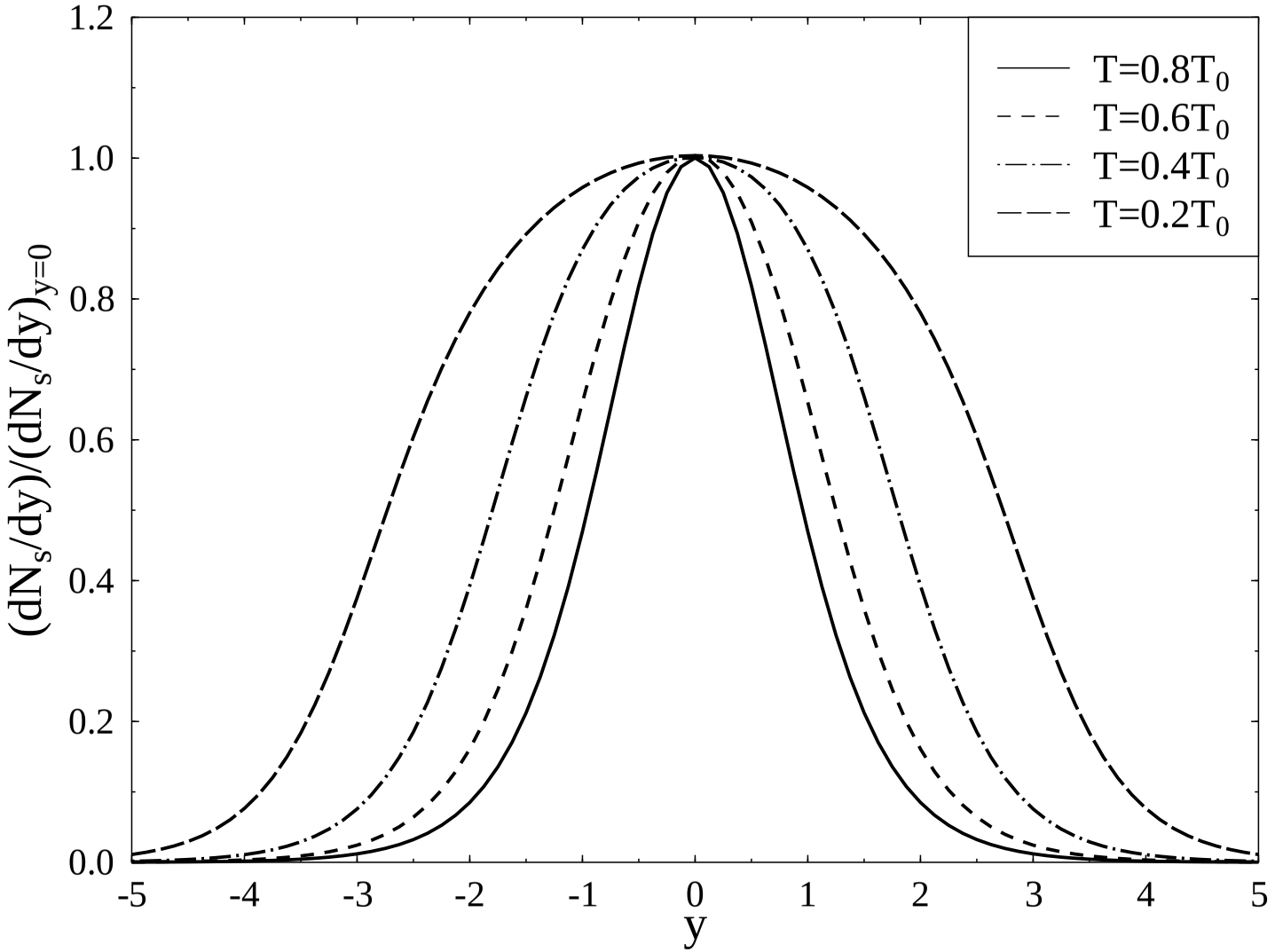
1.2
1.0
0.8
0.6
0.4
0.2
0.0
-5
-4
-3
-2
-1
0
1
2
3
4
5
y
$(dN_s/dy)/(dN_s/dy)_{y=0}$
T=0.8T0
T=0.6T0
T=0.4T0
T=0.2T0

fig.12